J Biol Inorg Chem (2014) 19:145–159
DOI 10.1007/s00775-013-1036-y

ORIGINAL PAPER

Dynamic aggregation of the mid-sized gadolinium complex $\{Ph_4[Gd(DTTA)(H_2O)_2]^-{}_3\}$

Hugues Jaccard · Pascal Miéville · Caroline Cannizzo · Cédric R. Mayer · Lothar Helm

Received: 3 July 2013 / Accepted: 14 August 2013 / Published online: 14 September 2013

Abstract A compound binding three Gd^{3+} ions, $\{Ph_4[Gd(DTTA)(H_2O)_2]^-{}_3\}$ (where H_5DTTA is diethylenetriaminetetraacetic acid), has been synthesized around a hydrophobic center made up of four phenyl rings. In aqueous solution the molecules start to self-aggregate at concentrations well below 1 mM as shown by the increase of rotational correlation times and by the decrease of the translational self-diffusion constant. NMR spectra recorded in aqueous solution of the diamagnetic analogue $\{Ph_4[Y(DTTA)(H_2O)_2]^-{}_3\}$ show that the aggregation is dynamic and due to intermolecular π-stacking interactions between the hydrophobic aromatic centers. From estimations of effective radii, it can be concluded that the aggregates are composed of two to three monomers. The paramagnetic $\{Ph_4[Gd(DTTA)(H_2O)_2]^-{}_3\}$ exhibits concentration-dependent ^1H NMR relaxivities with high values of approximately 50 mM^{-1} s^{-1} (30 MHz, 25 °C) at gadolinium concentrations above 20 mM. A combined analysis of ^1H NMR dispersion profiles measured at different concentrations of the compound and ^{17}O NMR data measured at various temperatures was performed using different theoretical approaches. The fitted parameters showed that the increase in relaxivity with increasing concentration of the compound is due to slower global rotational motion and an increase of the Lipari–Szabo order parameter S^2.

Keywords Gadolinium · Imaging agent · Relaxometry · Aggregation · π-stacking

Abbreviations

AFA	Anisotropic Florence approach
DO3A	Tetraazacylcododecanetriacetic acid
DOSY	Diffusion-ordered spectroscopy
DSS	4,4-Dimethyl-4-silapentane-1-sulfonic acid
ESI	Electrospray ionization
FFC	Fast field cycling
H_5DTTA	Diethylenetriaminetetraacetic acid
HPLC	High-performance liquid chromatography
MRI	Magnetic resonance imaging
MS	Mass spectrometry
NMRD	NMR dispersion
Ph_4DTTA_3	1,3,5-Tris{4-[(bis{2-[bis(carboxymethyl) amino]ethyl}amino)methyl]phenyl}benzene
RFB	Rast–Fries–Belorizky
SBM	Solomon–Bloembergen–Morgan
ZFS	Zero-field splitting

Introduction

The two last decades has seen tremendous effort and successful progress in the optimization of the efficiency of magnetic resonance imaging (MRI) T_1 contrast agents. Those paramagnetic compounds, constituted mainly by cyclic or acyclic gadolinium(III) chelate complexes, increase the relaxation rate of the water protons, the

Responsible Editor: Valerie C. Pierre.

Electronic supplementary material The online version of this article (doi:10.1007/s00775-013-1036-y) contains supplementary material, which is available to authorized users.

H. Jaccard · P. Miéville · C. Cannizzo · L. Helm (✉)
Institut des Sciences et Ingénierie Chimiques, Ecole Polytechnique Fédérale de Lausanne (EPFL), EPFL-BCH, 1015 Lausanne, Switzerland
e-mail: lothar.helm@epfl.ch

C. R. Mayer
Laboratoire d'Ingénierie des Systèmes de Versailles LISV-EA 4048, Université de Versailles Saint-Quentin-en-Yvelines, 10/12 Avenue de l'Europe, 78140 Vélizy, France

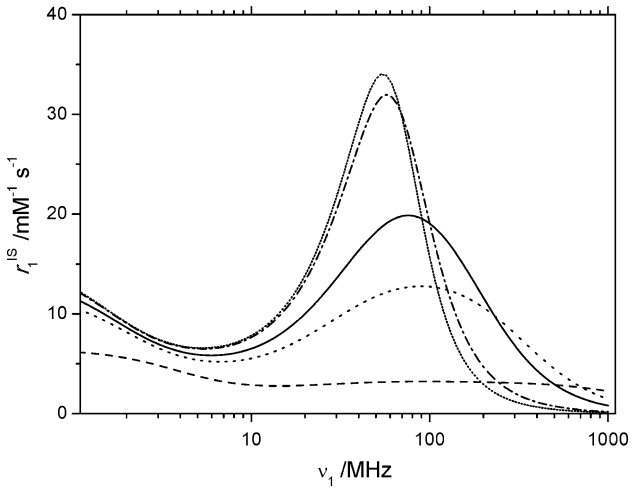

Fig. 1 Simulated effect of the rotational correlation time on the inner-sphere relaxivity r_1^{IS} as a function of the Larmor frequency, calculated by the Solomon–Bloembergen–Morgan theory for τ_R values of 0.1 ns (*dashed line*), 0.5 ns (*doted line*), 1 ns (*straight line*), 5 ns (*dash-dotted line*), and 10 ns (*short-dotted line*). Other parameters are as follows: $\tau_M = 100$ ns; $\tau_v = 10$ ps; $\Delta^2 = 0.5 \times 10^{20}$ s^{-2}; $q = 1$

parameter most commonly measured by MRI. The efficiency of contrast agents, described by the relaxivity r_1, depends on the electronic relaxation time of the metal center, on the number of water molecules in the inner sphere of the complex, on the exchange rate of these water molecules, and on the molecular size through the rotational correlation time τ_R. The latter is the predominant parameter between approximately 10 and 200 MHz, which a few years ago corresponded to the working frequency range of most medical MRI magnets (typically 1.5 T or 64 MHz) [1]. The efficiency of potential MRI contrast agents was therefore optimized through the development of large, slowly tumbling molecules (Fig. 1).

Developed to counteract the relative low sensitivity of MRI and thanks to technological progress, high-field magnets are nowadays available for human MRI analysis [1–3]. In magnetic fields higher than 4.7 T (200 MHz), the relaxivity of the big and slowly rotating compounds, and therefore their efficiency as potential contrast agents, drops drastically. In this field region the highest relaxivities are reached by molecules whose rotational correlation times typically range from 0.5 to 1 ns, inducing the development of mid-sized compounds as potential high-field contrast agents [4, 5]. To increase the density of relaxivity, many of them have several paramagnetic complexes bound to a central benzene [6–9] or metal [10–13] core. Within this framework, Costa et al. [6] described unusual systems, constituted by two DO3A^{3-} (1,4,7,10-tetraazacyclododecane-1,4,7-triacetate) chelating units linked via *meta* and *para* positions to a central xylene core, presenting exceptionally high relaxivities for mid-sized

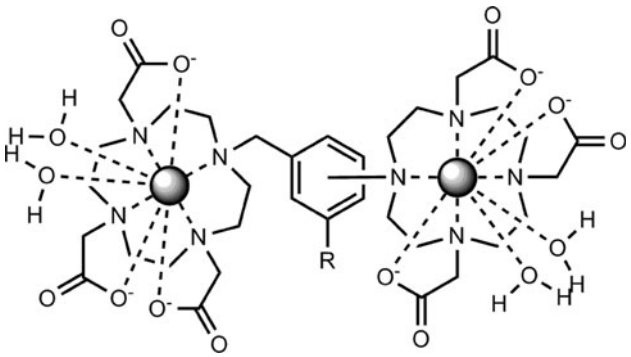

Fig. 2 Aggregating Gd^{3+} complexes described by Costa et al. [6] with R is H (DO3A in *meta* and *para* positions) and R is COOH (DO3A in the 3-*meta* and 5-*meta* positions)

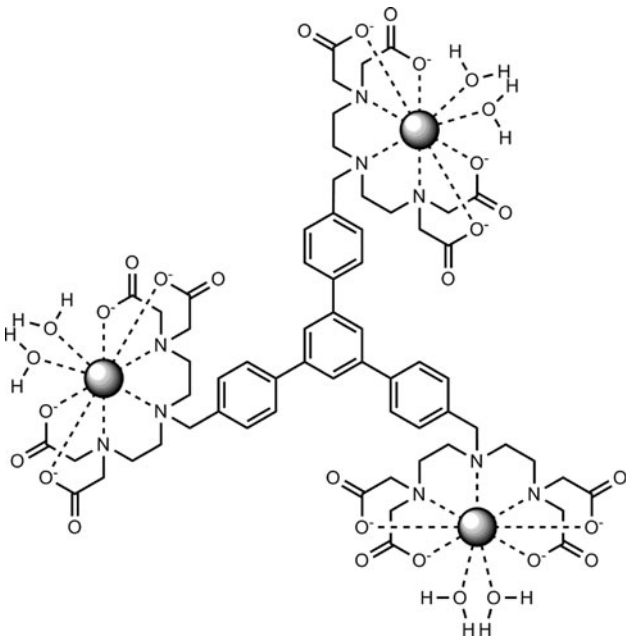

Fig. 3 The gadolinium(III) complex $\{Ph_4[Gd(DTTA)(H_2O)_2]^-{}_3\}$

molecules (Fig. 2). Self-aggregation, forming aggregates of about ten "monomers," was proved to be accountable for these unexpected relaxivities. As such aggregates have not been observed in nonaromatic dimeric Gd^{3+} complexes [14, 15], the intermolecular interactions result most probably from π-stacking of the aromatic core, although other hydrophobic interactions or hydrogen bonding cannot be excluded.

To investigate this aggregation phenomenon further, we describe here the gadolinium complex of the ligand 1,3,5-tris{4-[(bis{2-[bis(carboxymethyl)amino]ethyl}amino) methyl]phenyl}benzene (Ph_4DTTA_3; **5**), composed of three heptadentate DTTA (H_5DTTA is diethylenetriaminetetraacetic acid) chelating moieties around a central core constituted by four benzene rings (Fig. 3). The aromatic central core has been designed specially to induce the formation of aggregates by strong π-stacking

intermolecular interactions. The synthesis of the ligand, the relaxometric characterization of the Gd^{3+} complex, and investigations on the size of the aggregates and the nature of the intermolecular interactions are reported.

Materials and methods

Ligand synthesis and characterization

All chemicals were purchased from sources of high-quality chemicals (Sigma-Aldrich, Acros) and were used as received without purification.

^{1}H and ^{13}C NMR spectra were recorded with a Bruker DRX-400 spectrometer (9.4 T). Mass spectrometry (MS) analyses were performed with a Thermo Fischer TSQ7000 spectrometer using an electrospray ionization (ESI) ion source. High-performance liquid chromatography (HPLC) purifications were performed with a Dionex system made up of a UVD 170U detector and a P580 pump, using a SunFire™ Prep C_{18} OBD™ 5-μm column (19 mm × 150 mm). Elemental analyses were performed by Euro Solari at the Elemental Analysis Service at Institute of Chemical Sciences and Engineering, Swiss Federal Institute of Technology in Lausanne.

Synthesis of tert–butyl 2,2′,2″,2‴-[iminobis(ethane-2,1-diylnitrilo)]tetraacetate

tert–Butyl 2,2′,2″,2‴-[iminobis(ethane-2,1-diylnitrilo)]tetraacetate (**1**) was synthesized according to the literature [7, 16].

Synthesis of 1,3,5-tris(4-methylphenyl)benzene and 1,3,5-tris(4-bromomethylphenyl)benzene

1,3,5-Tris(4-methylphenyl)benzene (**2**) and 1,3,5-tris(4-bromomethylphenyl)benzene (**3**) were synthesized according to the literature [17–20].

Synthesis of 1,3,5-tris{4-[(bis{2-[bis(tert-butyl acetate)amino]ethyl}amino)methyl]phenyl}benzene

For the synthesis of 1,3,5-tris{4-[(bis{2-[bis(*tert*-butyl acetate)amino]ethyl}amino)methyl]phenyl}benzene (**4**), 1.83 g (3.27 mmol) of **1** was dissolved in 90 ml of dry dimethylformamide. Then, 608.7 mg (1.040 mmol) of **3**, dissolved in 10 ml of dry dimethylformamide, were added dropwise under an argon atmosphere. The reaction mixture was stirred overnight at 55 °C and evaporated to dryness. The residue was dissolved in 200 ml of dichloromethane and washed three times with 100 ml of water. The organic phase was dried over sodium sulfate and evaporated to dryness. The crude product was purified by silica gel chromatography (95:5 dichloromethane/methanol) (R_f = 0.19). Finally, 212 mg (yield 10 %) of pure compound **4** was obtained. ^{1}H NMR ($CDCl_3$, 400 MHz) δ (ppm): 1.43 (s, 108 H), 2.67 (t, *J* undetermined, 12 H), 2.87 (t, *J* undetermined, 12 H), 3.43 (s, 24 H), 3.70 (s, 6H), 7.41 (d, $J = 7.0$ Hz, 6 H), 7.61 (d, $J = 7.0$ Hz, 6 H), 7.74 (s, 3 H). MS (ESI) *m/z* (%): 675.1 (100) $[M + 3H]^{3+}$, 1,011.3 (5) $[M + 2H]^{2+}$.

Synthesis of Ph_4DTTA_3

For the synthesis of Ph_4DTTA_3 (**5**), 200 mg (99 μmol) of **4** was dissolved in 5 ml of a 5 % water in trifluoroacetic acid solution and the mixture was stirred for 3 h. The solvents were removed by evaporation and the residue was washed with 10 ml of water and evaporated to dryness five times. The resulting solid was dissolved in 12 ml of a 0.1 M triethylammonium acetate buffer and purified on a C_{18} preparative HPLC column, using 0.1 M triethylammonium acetate buffer and a 0–60 % in 30 min acetonitrile gradient as the elution system. The pure fractions, eluted after 15.0 min, were collected, evaporated, and washed until no triethylammonium acetate remained. Finally, 52 mg (39 μmol) of pure compound **5** was obtained (yield 39 %). ^{1}H NMR (D_2O, 400 MHz) δ (ppm): 2.99 (t, *J* undetermined, 12 H), 3.51 (t, *J* undetermined, 12 H), 3.69 (s, 24 H), 3.82 (s, 6 H), 7.54 (d, $J = 6.7$ Hz, 6 H), 7.80 (d, $J = 6.4$ Hz, 6H), 7.96 (s, 3 H). ^{13}C NMR (D_2O, 54.3 MHz) δ (ppm): 47.38 (CH_2–N), 52.12 (CH_2–N), 56.73 (CH_2-CO), 57.64 (Ar-CH_2–N), 124.89 (CHAr), 127.69 (CH–CHAr), 130.51 (CH–CHAr), 135.91 (CAr), 139.96 (CAr), 141.55 (CAr), 170.34 (CO). MS (ESI) *m/z* (%): 675.3 (100) $[M + 2H]^{2+}$, 1,349.5 (96) $[M + H]^{+}$. Elemental analysis. Calcd (%) for $[H_{15}Ph_4DTTA_3]^{3+}[Cl]^{-}{}_3$ ($C_{63}H_{84}Cl_3N_9O_{24}$) + 0.67 [$HNEt_3{}^{+}Cl^{-}$] ($C_6H_{15}ClN$; integration of ^{1}H NMR peak) ($C_{67.03}H_{94.09}Cl_{3.67}N_{9.67}O_{24}$; 1,549.64 g mol^{-1}): C 51.96, H 6.12, N 8.74. Found (%): C 52.15, H 6.05, N 8.64.

Sample preparation

Gadolinium complex

The solid salt $GdCl_3{\cdot}xH_2O$ ($x \approx 6.7$) was dissolved in H_2O to prepare the 60 mM Gd^{3+} stock solution. The exact ion concentration was measured by complexometric titration using 5.00 mM Na_2H_2EDTA. A 24.51 mM solution of **5** was prepared in H_2O, and the chelator concentration was determined by back titration of a Gd^{3+} excess with 5.00 mM Na_2H_2EDTA. The titrations were performed with a Metrohm 665 Dosimat, using xylenol orange as the complexometric indicator and buffered at pH 5.8 with a 5 % (w/v) hexamethylenetetramine solution in water. The

complex $\{Ph_4[Gd(DTTA)(H_2O)_2]^-{}_3\}$ was prepared by adding a slight deficit of Gd^{3+} (2 %) to the ligand solution. The pH was brought back to 5.8 with 0.1 M NaOH, and the absence of free gadolinium was checked by the xylenol orange test in 5 % (w/v) hexamethylenetetramine buffer. Finally, the exact final Gd^{3+} concentration was measured by means of the bulk magnetic susceptibility [21] at 23.3 °C with a Bruker DRX-400 (9.4 T, 400 MHz) spectrometer. This was done by measuring the shift of the *tert*-butanol alkyl protons in the paramagnetic environment compared with the diamagnetic aqueous reference contained in a coaxial NMR tube.

Yttrium complex

A 62 mM Y^{3+} stock solution was prepared by dissolving $YCl_3{\cdot}xH_2O$ ($x \approx 6$) in H_2O. The exact ion concentration was measured by complexometric titration using 5.00 mM Na_2H_2EDTA. A 10.85 mM solution of **5** was prepared in H_2O, and the chelator concentration was measured by back titration of a Gd^{3+} excess with 5.00 mM Na_2H_2EDTA. To ensure complete complexation, the $\{Ph_4[Y(DTTA)(H_2O)_2]^-{}_3\}$ complex was prepared by adding an excess of 2 % Y^{3+} to the ligand solution. The pH was brought back to 5.8 with 0.1 M NaOH, and the presence of free Y^{3+} was checked by the xylenol orange test in 5 % (w/v) hexamethylenetetramine buffer. The solution was evaporated to dryness, and the complex was recovered by dissolution in D_2O–0.1 % 4,4-dimethyl-4-silapentane-1-sulfonic acid DSS). The concentration of complexed yttrium, determined by the weight of D_2O added ($d_{D2O}{}^{23\ °C} = 1.1047$ g cm^{-3}) [22], was 4.20 mM. A dilute solution was prepared by dilution of the latter solution, and the concentration of complexed yttrium was determined by the weight of D_2O added as 92.6 μM.

^{1}H relaxivities

T_1 values were measured using the following equipment: a Stelar Spinmaster fast field cycling (FFC) NMR relaxometer [23] (2.35×10^{-4} to 0.47 T; ^{1}H Larmor frequencies of 0.01–20 MHz), Bruker minispec mq20 0.47 T (20 MHz), mq40 0.70 T (30 MHz), mq40 0.94 T (40 MHz), and mq60 1.41 T (60 MHz) instruments, a Bruker Avance 200 console connected to 2.35 T (100 MHz) and 4.7 T (200 MHz) cryomagnets, Bruker Avance II 9.4 T (400 MHz) and Bruker Avance 18.8 T (800 MHz) spectrometers. The temperature was controlled either by a thermostated gas flow (FFC, cryomagnets) or by pumping a thermostated liquid trough the probe (minispec). Sample tubes with an outer diameter of 7.5 mm were used for the mq40 and mq60 instruments, whereas samples sealed in glass spheres adapted for 10-mm NMR tubes were used for all other instruments. All temperatures were measured by substitution techniques [24]. The relaxivities r_1 (mM^{-1} s^{-1}) were calculated using Eq. 4 using diamagnetic relaxation contributions $1/T_1^{dia}$ of 0.366 and 0.326 s^{-1} for 25 and 37 °C, respectively.

NMR dispersion (NMRD) profiles of $\{Ph_4[Gd(DTTA)(H_2O)_2]^-{}_3\}$ were measured at 25.0 °C (0.101, 1.84, and 18.18 mM Gd^{3+}) and 37.0 °C (1.84 and 18.18 mM Gd^{3+}). T_1 of the most concentrated sample was too short (1 ms or less) to be measured by the FFC relaxometer; therefore, only data at Larmor frequencies of 20 MHz and above could be measured.

^{1}H NMR and ^{1}H diffusion-ordered spectroscopy NMR of $\{Ph_4[Y(DTTA)(H_2O)_2]^-{}_3\}$

All ^{1}H spectra of the concentrated and dilute $\{Ph_4[Y(DTTA)(H_2O)_2]^-{}_3\}$ solutions were measured at various temperatures (275, 285, 295, 305, 315, 325, 335, and 345 K) with a Bruker Avance II (18.8 T, 800 MHz) spectrometer equipped with a cryoprobe.

^{1}H diffusion-ordered spectroscopy (DOSY) spectra of $\{Ph_4[Y(DTTA)(H_2O)_2]^-{}_3\}$ for Y^{3+} concentrations of 4.3 mM (concentrated sample) and 0.1 mM (diluted sample) at various temperatures were acquired with a pulsed field gradient sequence [25] with HDO signal presaturation and were calibrated for chemical shift and diffusion with DSS. The DOSY spectra were acquired with a continuous-wave presaturation period of 4 s, 16 gradient steps, and 32 transients for the concentrated sample and 256 transients for the diluted sample. The acquisition of the spectra of the diluted sample required more than one night.

^{17}O NMR spectroscopy

Variable-temperature ^{17}O NMR measurements were performed with a Bruker Avance II 9.4 T (54.3 MHz) spectrometer, equipped with a Bruker BVT3000 temperature control unit and a Bruker BCU05 cooling unit. For these measurements, 10.5 % ^{17}O-enriched water (Irakli Gverdtsiteli Research and Technology Center on High Technologies and Super Pure Material) was added to the 18.2 mM sample to obtain a final 2 % ^{17}O enrichment and a 15.37 mM Gd^{3+} concentration. The sample was sealed in a glass sphere adapted for 10-mm NMR tubes to avoid susceptibility corrections to the chemical shifts. The chemical shifts and the transverse and longitudinal relaxation rates, using the inversion-recovery [26] and the Carr–Purcell–Meiboom–Gill [27] pulse sequences, respectively, were measured at 11 different temperatures in the range from −2 to 89.9 °C. The reduced relaxation rates T_{1r} and T_{2r} and the reduced chemical shift differences $\Delta\omega_r$, with respect to a pH 3.5 water reference (1 % ^{17}O enrichment), were

calculated using Eqs. 1, 2, and 3. Interpolated chemical shifts of the reference were used for the calculation of $\Delta\omega_r$. The number of water molecules in the inner sphere of the complex q was fixed to two.

$$\frac{1}{T_{ir}} = \frac{1}{P_M}\left(\frac{1}{T_i} - \frac{1}{T_i^{ref}}\right); \quad i = 1, 2 \tag{1}$$

$$\Delta\omega_r = \frac{1}{P_M}\left(\omega - \omega^{ref}\right) \tag{2}$$

with

$$P_M = \frac{q[M^{n+}]}{55.56} \tag{3}$$

Data treatment

For fits of the ^{1}H NMRD and ^{17}O NMR data, a Solomon–Bloembergen-based theory was used [28–30] supplemented with the Lipari–Szabo free-model approach for the internal rotation [31, 32] and the Rast–Fries–Belorizky (RFB) model for electronic spin relaxation [33, 34]. They were performed using Visualiseur/Optimiseur [35, 36] running on a MATLAB® 7.3.0 (R2006b) platform.

Fittings of the full NMRD profiles using the "anisotropic Florence approach" (AFA) [37–39] were performed with a program [40, 41] adapted to run on a PC under Windows 7.

The ^{1}H DOSY data were fitted with the T_1/T_2 analysis module of Bruker TopSpin 3.1.

Molecular modeling

The molecular modeling was performed by molecular mechanics using the MM3 force field [42–44] with Scigress Explorer^{TM} Ultra 7.7.0.47.

Results and discussion

Ligand synthesis

The use of the chelator DTTA presents many advantages. First, this acyclic poly(aminocarboxylate) is heptadentate, which allows there to be two water molecules in the inner sphere of the Gd^{3+} complex, and hence doubles its relaxivity. Then, the two water molecules in the complex are not adjacent, which prevents complexation with bidentate salts, such as carbonate typically, and allows skipping of degassing steps [45]. Finally, its synthesis using a succession of protection and deprotection is straightforward (four steps; Fig. 4) inexpensive, and leads to an acceptable global yield (40 %) [7]. Although its stability would not allow human applications, this chelating unit is stable enough for in vitro or animal in vivo studies [45]. The overall synthesis route of **5**, presented in Fig. 4, consists of three major steps: the synthesis of the DTTA chelating unit (**1**), the synthesis of the central core **3**, and their conjugation.

Compound **2** is formed with good yield through the triple condensation of 1-(4-methylphenyl)ethanone. The next step, the bromination of the methyl groups, using *N*-bromosuccinimide and benzoyl peroxide is more delicate. The exact stoichiometric quantity of *N*-bromosuccinimide is added dropwise in order to brominate every methyl position and avoid the massive formation of dibrominated methyl. The presence of side products, consisting of compound **3** with unsubstituted (–CH_3), disubstituted (–CH–Br_2), or hydroxylated (–CH_2–OH) methyl makes the purification of **3** arduous throughout the synthesis until the preparative HPLC purification.

The next step consists in the conjugation of the protected DTTA chelators on the three alkyl bromides of **3** in the presence of K_2CO_3 to obtain the protected Ph_4DTTA_3 (**4**). Chromatographic purification using a dichloromethane/methanol system was laborious owing to the bad separation of the side products. These impurities were essentially compound **4** with one unsubstituted methyl (–CH_3) or one hydroxymethyl (–CH_2–OH) arising from the hydroxylation of one unsubstituted bromide. This difficult purification, in addition to three S_N2 reactions on the same molecule, explains the unexpected low yield (10 %) obtained.

Finally, the *tert*-butyl protecting groups were removed by trifluoroacetic acid to obtain the free acid Ph_4DTTA_3 (**5**). The purification of this compound, which precipitates in aqueous solutions with pH lower than 3, was again laborious. Bio-Rad AG 50W-X4 cationic exchange resin, commonly used to purify poly(amino carboxylates), could not be used, and Bio-Rad AG 1-X4 anionic exchange resin and Sephadex LH-20 size-exclusion resin were inefficient. The purification was finally made possible by preparative HPLC, using water with 0.1 M triethylammonium acetate as a buffer and ion-pairing agent in a water/acetonitrile system. ESI–MS analyses were performed with pure methanol without formic acid to prevent precipitation in the capillary. Eventually, compound **5** was isolated in eight steps with an overall yield of 2 %.

Effect of concentration on the relaxivity

Early measurements of relaxivity revealed exceptionally high values for a mid-sized molecule. We therefore measured the relaxivity of $\{Ph_4[Gd(DTTA)(H_2O)_2]^-{}_3\}$ as a function of concentration. Relaxivity, r_1, is commonly defined as the increase in nuclear spin relaxation normalized to 1 mM concentration of the paramagnetic ion (Eq. 4):

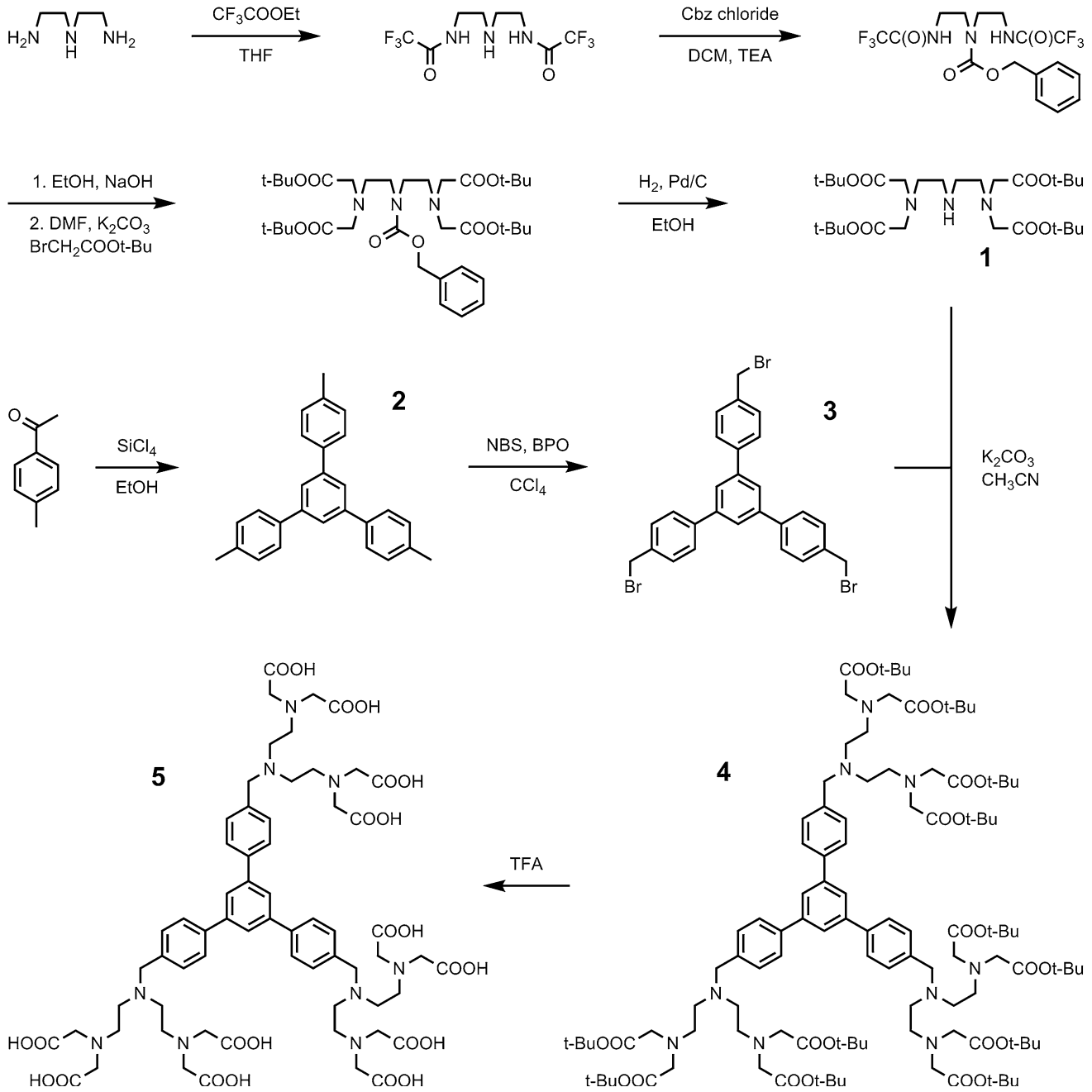

Fig. 4 Synthesis of Ph_4DTTA_3 (**5**). *BPO* benzoyl peroxide, *Cbz* carbobenzoxy, *DCM* dichloromethane, *DMF* dimethylformamide, *NBS* *N*-bromosuccinimide, *TEA* tetraethylammonium, *THF* tetrahydrofuran

$$r_1 = \frac{1}{[Gd^{3+}]}\left(\frac{1}{T_i} - \frac{1}{T_i^{dia}}\right) \quad \text{with } [Gd^{3+}] \text{ in mM} \tag{4}$$

where the Gd^{3+} concentration is in millimoles per liter.

The data reported in Fig. 5 show that the relaxivity almost doubles if the Gd^{3+} concentration is raised from 0.01 mM to approximately 20 mM. As the electron spin relaxation rate, the water exchange rate constant, and the number of molecules in the inner sphere of Gd^{3+} are supposed to be unaffected by the concentration, the observed concentration dependence of r_1 has to be induced by a variation of the rotational correlation time τ_R. In the simple Stokes–Einstein–Debye model, τ_R is related to the viscosity of the solution, η, and the size of the molecule characterized by an effective radius r (Eq. 5) [46]:

$$\tau_R = \frac{4\pi r^3 \eta}{3k_B T} \tag{5}$$

At Gd^{3+} concentrations of 20 mM and below (or less than 7 mM $\{Ph_4[Gd(DTTA)(H_2O)_2]^-_3\}$), the viscosity will stay

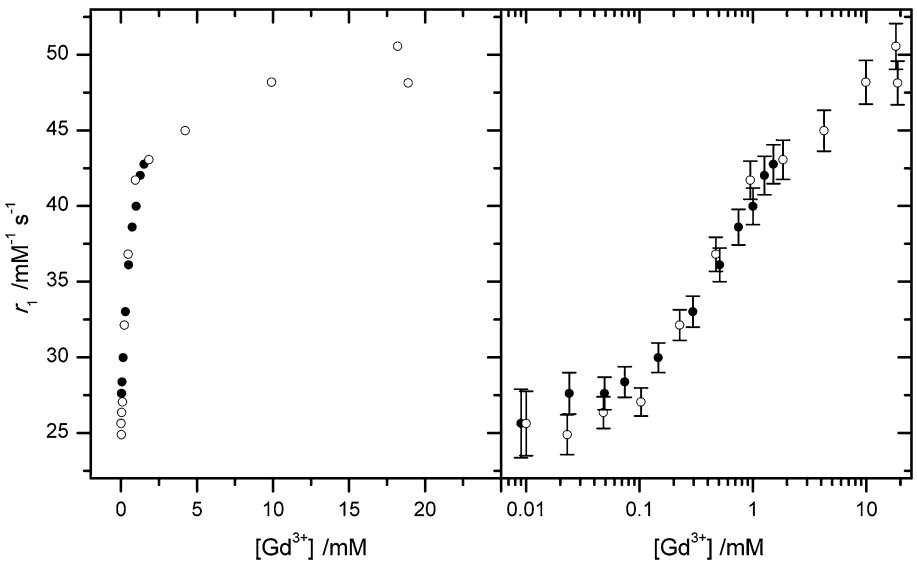

Fig. 5 Concentration-dependent relaxivities r_1 on linear (*left*) and log (*right*) scales, measured at 30 MHz and 25 °C on two different batches of $\{Ph_4[Gd(DTTA)(H_2O)_2]^-{}_3\}$ (*black circles* and *white circles*). *Error bars* refer to relative errors of 3 % on $1/T_1$ and $1/T_1^{dia}$

constant and the increase in τ_R can be attributed to an increase in the size of the rotating entity. The formation of dynamic intermolecular aggregates increasing the rotational correlation time is probably the only way to explain the high relaxivities and their concentration dependence.

From the sigmoid shape observed in the logarithmic plot (Fig. 5, right), one finds a relaxivity of approximately 25 mM^{-1} s^{-1} (25 °C, 30 MHz) at concentrations below 0.05 mM Gd^{3+}. At concentrations above 10 mM, the relaxivity measured is close to 50 mM^{-1} s^{-1}.

To investigate further the observed change in relaxivity, NMRD profiles were measured at concentrations of 0.10, 1.84, and 18.2 mM, corresponding to three distinct regions in the sigmoid curve (Fig. 5). All three profiles show a relaxivity hump at Larmor frequencies between 10 and 100 MHz. This r_1 hump markedly increases with the concentration of the compound (Fig. 6), indicating slower rotational diffusion at higher concentrations.

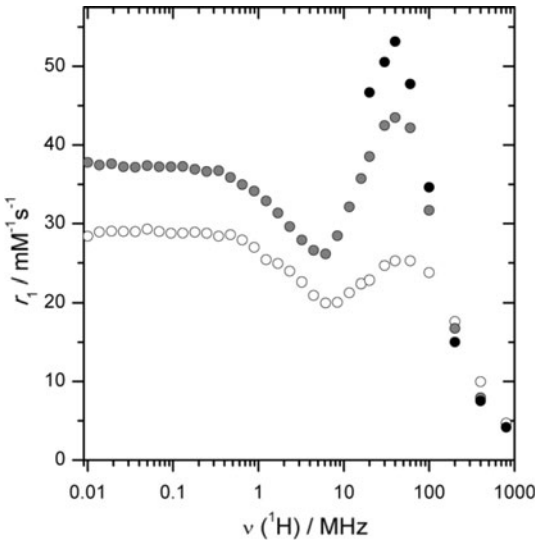

Fig. 6 ^{1}H NMR dispersion (NMRD) profiles of $\{Ph_4[Gd(DTTA)(H_2O)_2]^-{}_3\}$ measured at 25 °C for 0.101 mM Gd^{3+} (*white circles*), 1.84 mM Gd^{3+} (*gray circles*), and 18.2 mM Gd^{3+} (*black circles*)

Theoretical models used for data fitting

To extract quantitative results for the three dynamic processes governing the ^{1}H NMRD profiles, namely, rotational diffusion (correlation time τ_R), residence time for inner-sphere water molecules ($\tau_M = 1/k_{ex}$, with k_{ex} being the water exchange rate constant), and electron spin relaxation times (T_{1e} and T_{2e}), a combined analysis of data from ^{17}O NMR and ^{1}H NMRD measurements leads, in general, to the most reliable results [47]. Oxygen-17 transverse relaxation $1/T_{2r}$ is mostly governed by water exchange and gives, therefore, directly k_{ex}. Oxygen-17 longitudinal relaxation $1/T_{1r}$ is linked to the rotational diffusion of the vector linking the paramagnetic center Gd^{3+} to the inner-sphere water molecule(s). Because ^{17}O NMR is generally measured at high magnetic fields, 9.4 T in our case, the simple Solomon–Bloembergen–Morgan (SBM) theory is, in general, a good approximation, and data fitting is relatively simple.

The theoretical calculation of ^{1}H NMRD profiles is more complex. The "outer-sphere" contribution due to water molecules diffusing freely in the vicinity of the complex is mostly described by equations developed by Hwang and Freed [48, 49] and Ayant et al. [50]. Different theoretical approaches have been developed to describe the more important contribution to r_1 due to inner-sphere water molecules [51]. The main difficulties in calculating r_1 due to inner-sphere water molecules arise in the case of slowly

rotating compounds and from to the failure of the Redfield approximations for the description of the electron spin relaxation.

To obtain the most reliable description of the rotational motion of $\{Ph_4[Gd(DTTA)(H_2O)_2]^-{}_3\}$ in aqueous solution, we decided to proceed in the following way. First, we included in all fittings the possibility of internal motion besides the global rotation of the compound. The model-free description of Lipari and Szabo was used [31, 32, 52]. Second, we performed a combined analysis of the ^{17}O data and the high-field part of the ^{1}H NMRD profiles, both measured on the concentrated solution (18.2 mM Gd^{3+}). Reliable ^{17}O NMR data could only be obtained at that high concentration of the paramagnetic compound. We chose the description of the electron spin relaxation developed by Rast et al. [34] and others in the frame of Redfield's approximations. From this treatment, the water exchange rate constant as well as the first global and local rotational correlation times were obtained. Third, fits of the NMRD profiles measured at three different Gd^{3+} concentrations were performed using three different theoretical descriptions. The first one was the simple SBM model. Because of the limited validity of the model, only data points at frequencies above 10 MHz were included in the fitting. In the second theoretical description, we used the RFB method as in the combined analysis which includes ^{17}O data. In this treatment, also only high-frequency data are fitted. The last theoretical description is based on the slow-rotation model developed in the group of Bertini [37, 53] in Florence. We used a modified version of the Florence program which includes the Lipari–Szabo model for internal motion (APA) [41]. This model allowed us to fit the full NMRD profiles, including low-frequency data.

^{17}O NMR and ^{1}H NMRD

Reduced ^{17}O transverse and longitudinal relaxation rates, $1/T_{2r}$ and $1/T_{1r}$, respectively, reduced chemical shifts, $\Delta\omega_r$, and high-field ^{1}H NMRD data are shown in Fig. 7 together with the curves obtained by the fitting. To obtain meaningful correlation times for the global and the internal motion, it was essential to extend the NMRD profiles to frequencies up to 800 MHz.

The simultaneous fitting of the data acquired for the 18.2 mM sample was performed using two theoretical approximations, the SBM model and the RFB model. Both led to fits of comparable quality and similar common parameters. The two models differ mainly in the description of electron spin relaxation, and therefore the parameters describing this dynamic process are different (Table 1). To obtain an acceptable combined fit of ^{17}O and

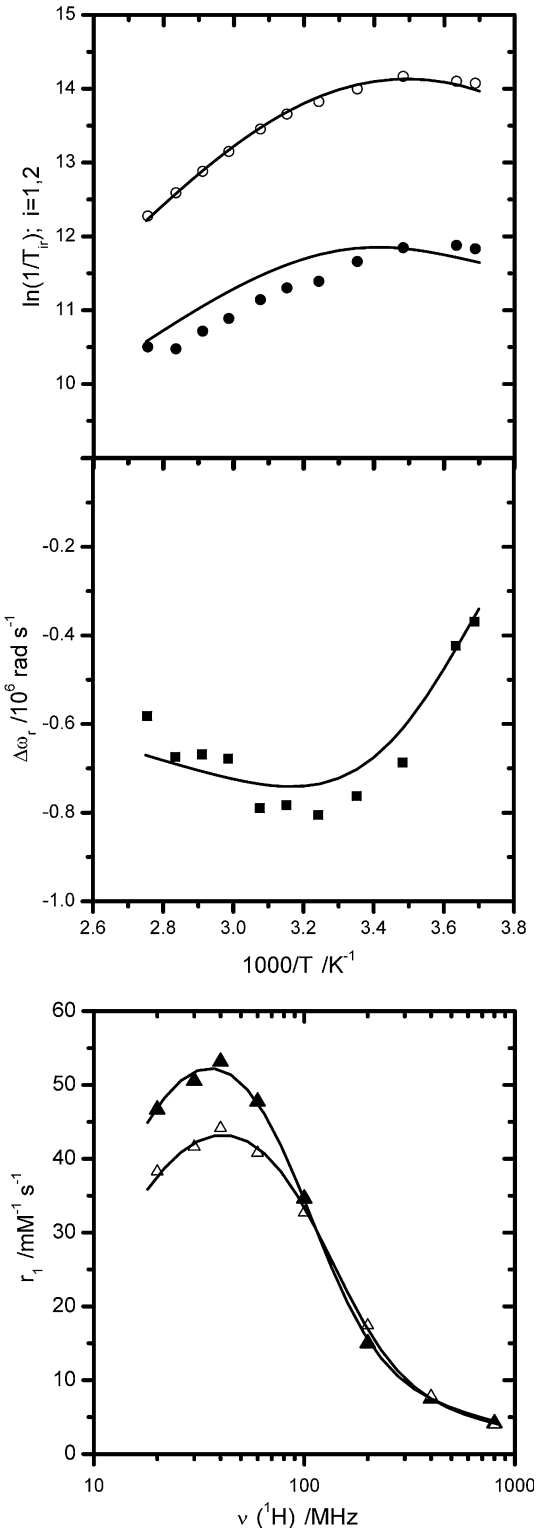

Fig. 7 Simultaneous best fits of the ^{17}O NMR data [ln $1/T_{1r}$ (*black circles*), ln $1/T_{2r}$ (*white circles*), and $\Delta\omega_r$ (*black squares*)] and the ^{1}H NMRD profiles [at 25 °C (*black triangles*) and 37 °C (*white triangles*)] of concentrated $\{Ph_4[Gd(DTTA)(H_2O)_2]^-{}_3\}$ [18.2 mM Gd^{3+}, Rast–Fries–Belorizky (RFB) model]

Table 1 Best-fit parameters of ^{17}O NMR and ^{1}H NMR dispersion (NMRD) data using the Solomon–Bloembergen–Morgan (*SBM*) model, the Rast–Fries–Belorizky (*RFB*) model, and the anisotropic Florence approach (*AFA*) for $\{Ph_4[Gd(DTTA)(H_2O)_2]^-{}_3\}$ (H_5DTTA is diethylenetriaminetetraacetic acid) for 0.101, 1.84, and 18.2 mM Gd^{3+}; fixed values are *italicized*

Parameters [Gd^{3+}]	SBM model	RFB model			AFA[a]		
	18 mM Gd^{3+}	18 mM Gd^{3+}	1.8 mM Gd^{3+}	0.10 mM Gd^{3+}	18 mM Gd^{3+}	1.8 mM Gd^{3+}	0.10 mM Gd^{3+}
$\Delta H^{\ddagger}$ (kJ mol^{-1})	37.7 ± 6.8	39.9 ± 8	*39.9*	*39.9*	*39.9*	*39.9*	
k_{ex}^{298} (10^6 s^{-1})	17.9 ± 5.6	17.0 ± 5	*17*	*17*	*17*	*17*	*17*
E_R (kJ mol^{-1})	21.8 ± 2	26.8 ± 6	*26.8*	*26.8*	14.7	22.3	–
τ_R^{298} (ps)	1,890 ± 78	2,770 ± 628	1,987 ± 99	817 ± 100	1,590	1,340	610
E_I (kJ mol^{-1})	18 ± 12	18 ± 5	*18*	*18*	*18*	*18*	*18*
τ_l^{298} (ps)	150 ± 242	197 ± 320	*197*	*197*	*197*	*197*	*197*
S^2	0.63 ± 0.02	0.61 ± 0.02	0.54 ± 0.02	0.47 ± 0.05	*0.61*	*0.54*	*0.47*
E_v (kJ mol^{-1})	*1*	*1*	*1*	*1*	*12.53*	*12.5*	*12.53*
τ_v^{298} [b](ps)	10 ± 2/0.7 ± 13	0.76 ± 0.2	*0.756*	*0.756*	*51.7*	*51.7*	*51.7*
$A/\hbar$ (10^6 rad s^{-1})	−3.8 ± 0.6	−3.7 ± 0.7	–	–			
τ_R^{HW}/τ_R^{OWb}	0.8 ± 1.3	0.9 ± 1.4	–	–			
Δ^2 [d] (10^{20} s^{-2})	0.082 ± 0.006/0.25 ± 2.2	–	–	–			
a_2 (10^{10} s^{-1})	–	0.88 ± 0.7	*0.88*	*0.88*	*0.798*[e]	0.798[e]	*0.798*[e]
a_4 (10^{10} s^{-1})	–	*0*	*0*	*0*			
a_6 (10^{10} s^{-1})	–	*0*	*0*	*0*			
a_{2T} (10^{10} s^{-1})	–	0.52 ± 0.12	*0.52*	*0.52*[c]	*0.419*[e]	0.419[c]	*0.419*[c]

[a] The AFA program does not give statistical errors.

[b] τ_R^{HW} is the rotational correlation time of the Gd–H_{water} vector and τ_R^{OW} is the rotational correlation time of the Gd–O_{water} vector (see [54, 55])

[C] Negative scalar coupling constants of similar size are, in general, observed for Gd^{3+} complexes [47, 56]

[d] Values for ^{1}H NMRD and ^{17}O NMR, respectively

[e] Converted from per centimeter to per second with $2\pi c$

^{1}H data using the SBM model we had to use different parameters for electron spin relaxation (τ_v, Δ^2) for ^{17}O and ^{1}H NMRD, otherwise the relaxivities measured at 60 MHz and below could not be fitted. The more elaborate RFB model, which includes a static contribution to zero-field splitting (ZFS), allowed a combined fit using the same parameters for ^{17}O and ^{1}H NMRD (Table 1).

NMRD profiles of the samples with lower Gd^{3+} concentrations (0.101 and 1.84 mM) were fitted using the RFB model with identical parameters, except the global rotational correlation time τ_R and the Lipari–Szabo order parameter S^2 (Fig. 8, left, Table 1). The RFB approach is not suitable for slowly tumbling molecules in low magnetic fields, and fitting performed on the whole profile would inexorably lead to erroneous τ_R^{298} values [57]. Therefore, only relaxivities from 16 to 800 MHz were included in the fitting. The remarkably good fits obtained by varying only the rotational correlation times and the Lipari–Szabo factor is further evidence that only the size of the molecule is responsible for the concentration-dependent relaxivities.

Finally, we fitted the same NMRD profiles measured at all three concentrations using the AFA. This model considers also a static and a transient ZFS, but assumes slow reorientation of the complex and no correlation between the rotation and translation of the complex and the electronic spin dynamics [38]. The program we used was modified with respect to the original version to include internal rotation described by the Lipari–Szabo model [41]. In contrast to the RFB model, the AFA allows one to fit the full NMRD profiles down to the lowest frequencies measured.

Good fits with the AFA were obtained by using the water exchange ($k_{ex} = 1/\tau_M$ and $\Delta H^{\ddagger}$) and internal rotation (τ_l, E_l, and S^2) parameters obtained from the RFB fits. Parameters for electron spin relaxation (E_v, τ_v, Δ, and D) were obtained from the full NMRD profiles measured at a concentration of 1.8 mM (Table 1). The same values were then used to fit the profiles measured at low (0.10 mM) and high (18 mM) concentrations. The only free parameter in these fits was the global rotational correlation time. The fits obtained are surprisingly good (Fig. 8, right).

Summarizing the data fitting, we can assert that the fitted parameters describing water exchange and global and

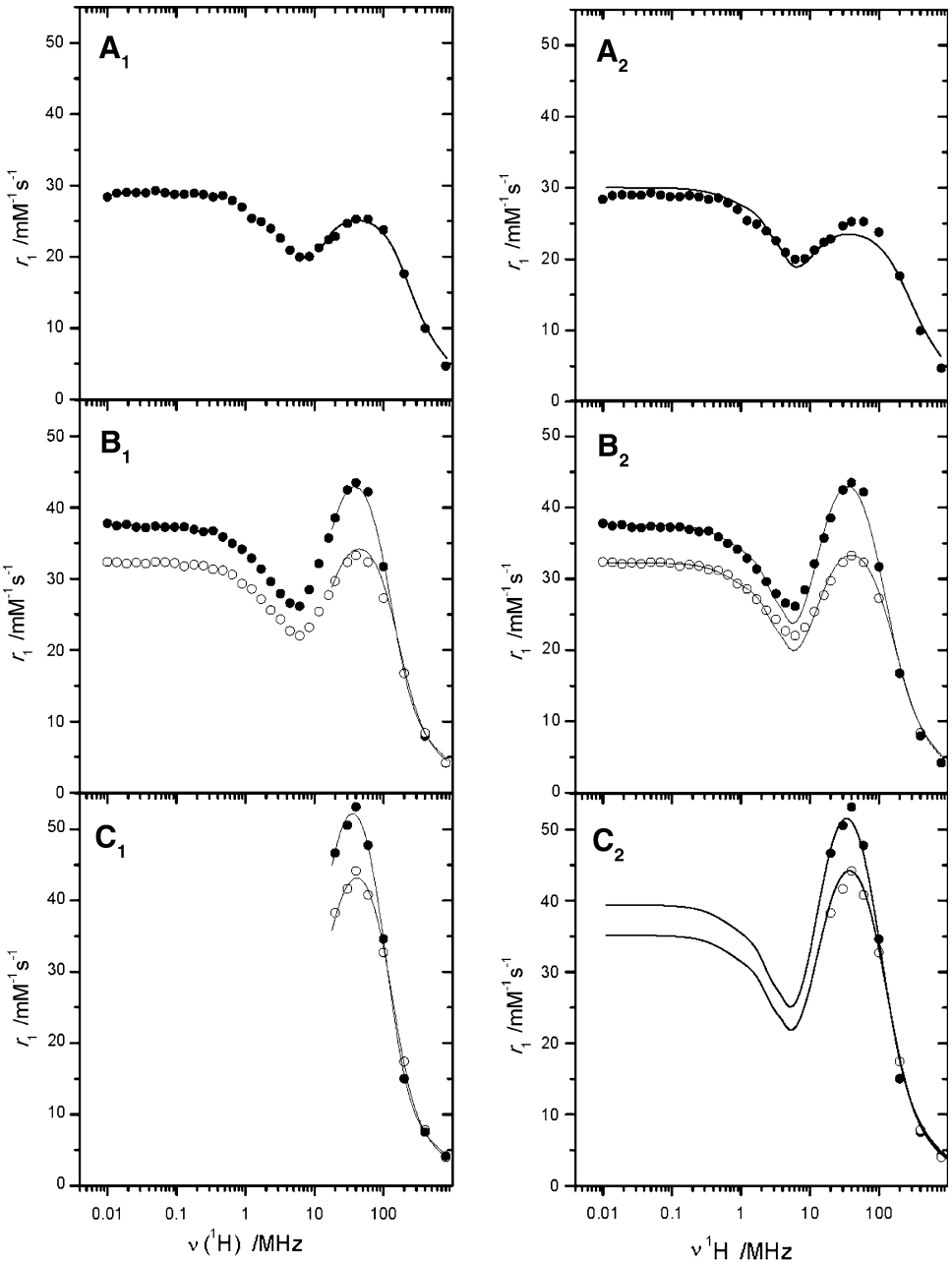

Fig. 8 NMRD profiles of $\{Ph_4[Gd(DTTA)(H_2O)_2]^{-}{}_3\}$ at 25 °C (*black circle*) for 0.101 mM (A_1, A_2), at 25.0 °C (*black circles*) and 37.0 °C (*white circles*) for 1.84 mM (B_1, B_2), and at 25.0 °C (*black circles*) and 37.0 °C (*white circles*) for 18.2 mM (C_1, C_2). The curves shown were calculated with the RFB model (*left*) and the anisotropic Florence approach (*right*)

internal rotational motion are independent of the theoretical model used. The only parameter varying as a function of concentration is the global rotational correlation time, τ_R.

The parameters describing electron spin relaxation depend on the model used. The simple SBM model uses only transient ZFS as a mechanism for electron spin relaxation, and the parameters τ_v and Δ^2 should be regarded as fitting parameters without deep physical meaning. The more elaborate RFB model and the AFA both include static and transient ZFS. Despite the differences in the models, surprisingly similar values for the static and transient ZFS were obtained. The correlation times for the transient ZFS, τ_v, differ, however, by almost two orders of magnitude.

The water exchange rate constant obtained is about twice as big as that of the dinuclear compound studied earlier ($k_{ex}^{298} \sim 9 \times 10^6\ s^{-1}$) [58]. The exchange rate constant was been obtained from ^{17}O data from a sample showing aggregation. The ^1H NMRD profiles are not very sensitive to k_{ex}; therefore, we cannot confirm that the monomers exhibit the same exchange rate constant. The relatively fast water exchange is not a limiting factor for relaxivity, as confirmed by the temperature dependence of r_1 observed for all samples studied (Fig. 8).

The most interesting parameters obtained are those describing rotational diffusion. Good fits could only be obtained by including a local motion. The rotational correlation time for this motion, τ_l, is approximately 200 ps, a value which suffers from high statistical uncertainty. Both fitting models applied clearly show that the global rotational correlation time, τ_R, decreases from more than 1.5–0.6 ns by dilution of the compound. At the same time, the Lipari–Szabo order parameter S^2, which describes the degree of internal motion in the compound, decreases from 0.6 to less than 0.5. This indicates that the compound has a higher degree of internal motion at lower concentrations. All these observations strongly support the formation of aggregates of complexes in solution at higher concentrations. The aggregated compounds rotate more slowly than the monomers; furthermore, they exhibit less internal motion because of mutual hindrance. In our fits we assumed the outer-sphere contribution to relaxivity to be independent of the concentration. Although the outer sphere does not affect the relaxation of ^{17}O, it has a non-negligible effect on the proton T_1 and therefore on the NMRD profile and the fitting.

High-resolution ^1H NMR and DOSY

The way the monomeric complexes interact to form bigger entities can be investigated by recording the ^1H NMR spectra of the diamagnetic analogue $\{Ph_4[Y(DTTA)(H_2O)_2]^-{}_3\}$. The paramagnetic ion Gd^{3+} is ideally replaced by Y^{3+} because of the same electric charge, similar ionic radius, and similar chemical properties of the two ions. The aromatic part of the ^1H NMR spectrum of $\{Ph_4[Y(DTTA)(H_2O)_2]^-{}_3\}$ contains (Fig. 9) essentially three signals, a singlet due to the three protons of the central phenyl (a in Fig. 9) and two multiplets (b in Fig. 9) due to the protons of the three external phenyls (Fig. 3). In the spectra we can also observe aromatic signals from the free form of the ligand (c in Fig. 9) and an impurity (d in Fig. 9). These last two signals were used in addition to the signal from DSS (not visible in Fig. 9) to calibrate the diffusion dimension in the further DOSY spectra.

Two main differences are striking on comparison of the spectrum of a dilute solution of $\{Ph_4[Y(DTTA)(H_2O)_2]^-{}_3\}$ (0.1 mM in D_2O) with that of a more concentrated one (4.3 mM in D_2O), both measured at 305 K: the resonances for the concentrated solution are shifted to lower frequencies and are markedly broadened (Fig. 9). The other chemical shifts of resonances from the aliphatic region (not shown in Fig. 9) and from spurious signals from the free form of the ligand as well as a small aromatic impurity are virtually identical. This observation confirms the presence of interaction between the π systems in aqueous solution.

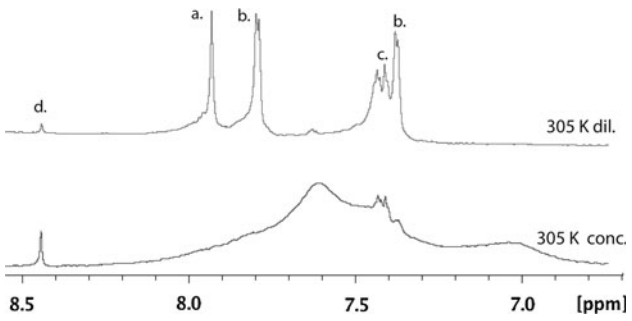

Fig. 9 Aromatic region of ^1H NMR spectra of a dilute (0.1 mM; *top*) and a concentrated (4.3 mM; *bottom*) solution of $\{Ph_4[Y(DTTA)(H_2O)_2]^-{}_3\}$ in D_2O measured at 800 MHz. Peak *a* corresponds to the central aromatic protons (see Fig. 3), peaks *b* are related to external aromatic rings, peaks *c* come from aromatic protons of the free form of the ligand, and peak *d* correspnds to an impurity. Chemical shifts were calibrated with respect to 4,4-dimethyl-4-silapentane-1-sulfonic acid

The broadening of the signals in the concentrated solution (Fig. 9, bottom) can be attributed to a kinetic effect.

The aggregates formed at higher concentrations are not inert entities: the complexes are converting between different aggregated forms and the monomeric form. To further strengthen this observation, a variable-temperature study was performed on the more concentrated solution. The very broad resonances found at the lowest temperature (275 K) continue to broaden, and coalesce at about 295 K. Further increase of temperature leads to narrowing of the coalesced signals (Fig. 10). This behavior is typical for systems undergoing chemical exchange.

Quantitative evaluation of the NMR spectra was not possible because no limiting spectrum with the absence of exchange was observed. Even more, when the temperature was increased, not only the exchange is accelerated but also the equilibria between the monomeric form and aggregates of different sizes change. Entropy will favor the dissociation of the aggregates at higher temperature.

To obtain further information on the formation of aggregates, 2D ^1H DOSY spectra [59] were obtained at 285, 305, and 325 K for the concentrated solution (4.3 mM) and at 305 K for the dilute solution (0.1 mM). The self-diffusion constants, D, measured are reported in Table 2. The diffusion constants were obtained through a selective fit using the TopSpin T_1/T_2 analysis module.

DSS and the impurity (d in Fig. 9) were used to calibrate the chemical shift and the diffusion measurements over the different temperatures. For both, an increasing self-diffusion constant, D, is observed for increasing temperature, as expected, mainly due to the decrease of viscosity. The apparent particle radius, r, calculated from Eq. 6,

$$D = \frac{k_B T}{6\pi\eta r} \tag{6}$$

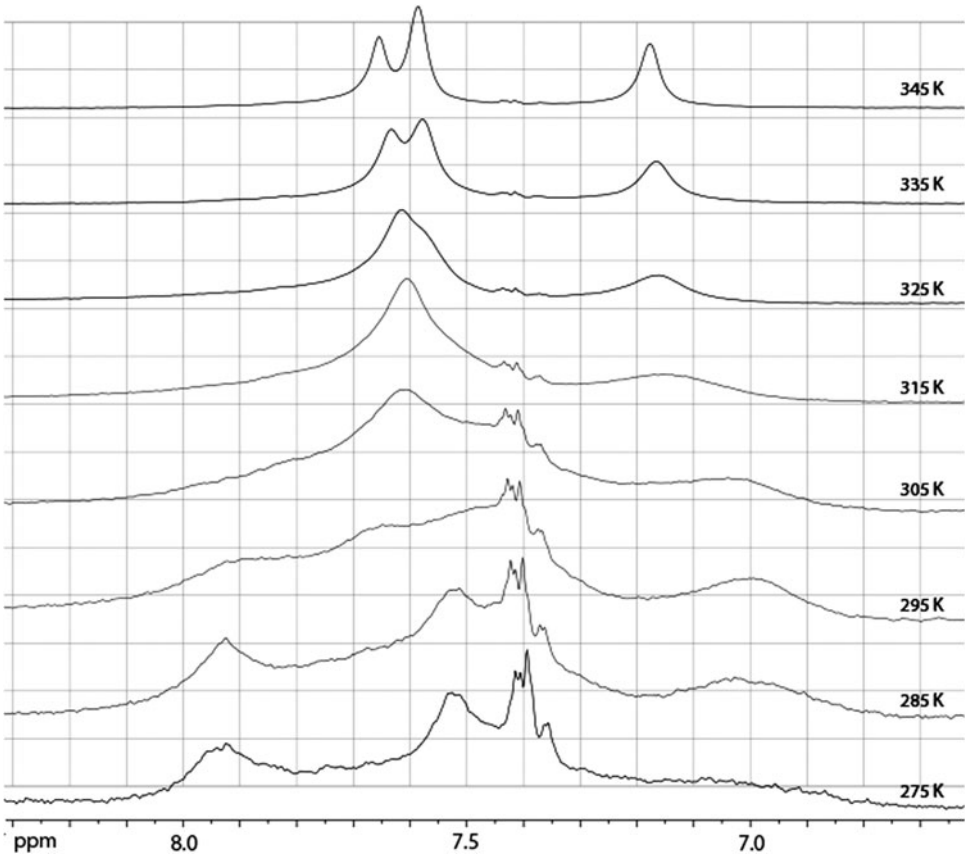

Fig. 10 Aromatic region of ^{1}H NMR spectra of a concentrated (4.3 mM) solution of $\{Ph_4[Y(DTTA)(H_2O)_2]^-{}_3\}$ in D_2O measured at various temperatures at 800 MHz; intensities are not conserved

Table 2 Translational diffusion constants of $\{Ph_4[Y(DTTA)(H_2O)_2]^-{}_3\}$ for 4.3 mM Y^{3+} (concentrated sample) and 0.1 mM Y^{3+} (diluted sample) measured by ^{1}H diffusion-ordered spectroscopy (DOSY) at various temperatures

T (K)	log D (m^2 s^{-1})/r (Å)				
	Aromatic region	Nonaromatic region	Free form of the ligand	Impurity	DSS
Concentrated sample (4.3 mM)					
285	–[a]	−10.17/20 ± 3	−9.71/6.8 ± 0.9	−10.71/2.4 ± 0.3	−9.40/3.3 ± 0.4
305	−9.70/12 ± 2	−9.70/12 ± 2	−9.31/5.0 ± 0.6	−9.00/2.4 ± 0.3	−9.15/3.4 ± 0.3
325	−9.15/5.4 ± 0.7	−9.70/6.4 ± 0.8	−9.06/4.4 ± 0.6	–	−8.90/3.0 ± 0.4
Diluted sample (0.1 mM)					
305	−9.56/8.8 ± 1.1	−9.61/10 ± 1.2	−9.12/3.2 ± 0.4	–	−9.09/2.9 ± 0.4

DOSY spectra were acquired with a pulsed field gradient sequence [60] with HDO signal presaturation and were calibrated with 4,4-dimethyl-4-silapentane-1-sulfonic acid (DSS). Diffusion constants were fitted using the TopSpin T_1/T_2 analysis module. On the basis of the measured diffusion constants, estimated radii were calculated using the Stokes–Einstein equation (Eq. 6)

[a] The aromatic region at 285 K is not measurable owing to the large broadening produced by the stacking

is constant within experimental error, confirming that the molecules do not aggregate in solution. The self-diffusion constants measured for $\{Ph_4[Y(DTTA)(H_2O)_2]^-{}_3\}$ in the concentrated solution from the NMR signals of the aromatic and the nonaromatic regions of the spectrum are smaller than those of the free form of the ligand and also those measured in the dilute solution. This slowing down of the translational motion can again be explained by formation of aggregates between the molecules in more concentrated solution.

As a general trend, larger apparent radii are observed for $\{Ph_4[Y(DTTA)(H_2O)_2]^-{}_3\}$ in concentrated solution compared with dilute solution (at constant temperature). From the small increase in r, it can be concluded that the aggregates are composed of two or at most three molecules. The apparent particle radius estimated for

Table 3 Mean radii of $\{Ph_4[M(DTTA)(H_2O)_2]^{-}{}_3\}$ agglomerates at various concentrations and 298 K estimated using the Stokes–Einstein–Debye equation (Eq. 5) in comparison with estimated radii established by DOSY at 305 K using the Stokes–Einstein equation (Eq. 6)

Fitting method		Metal concentration (mM)			
		18	4.3	1.8	0.10
Rotational diffusion (298 K); metal is gadolinium					
RFB model	*r* (Å)	15		13	10
AFA	*r* (Å)	12		11	9
Translational diffusion (305 K); metal is yttrium					
D	*r* (Å)		12		9

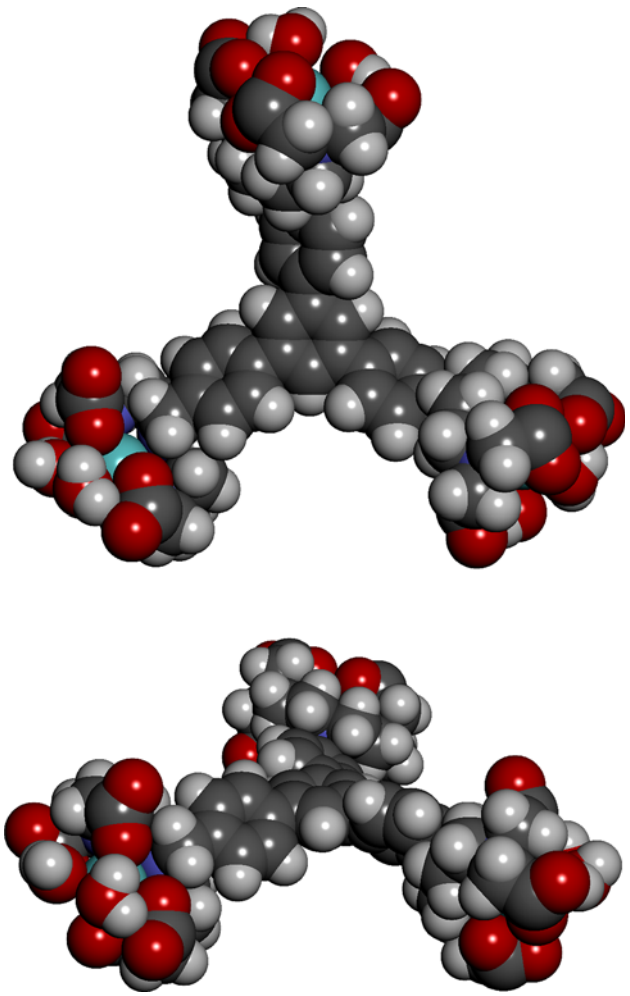

Fig. 11 MM3 molecular modeling of the $\{Ph_4[Gd(DTTA)(H_2O)_2]^{-}{}_3\}$ complex: *top* top view; *bottom side view*

$\{Ph_4[Y(DTTA)(H_2O)_2]^{-}{}_3\}$ decreases with increasing temperature, confirming that the equilibrium between monomers and aggregates is shifted towards monomers at higher temperatures.

Apparent particle radii can be obtained from rotational diffusion and from translational diffusion using either the Stokes–Einstein–Debye equation (Eq. 5) or the Stokes–Einstein equation (Eq. 6). A comparison of the *r* values obtained by both methods (Table 3) shows that the results are compatible. The formation of small aggregates between $\{Ph_4[Y(DTTA)(H_2O)_2]^{-}{}_3\}$ complexes was confirmed by both methods. One should keep in mind that both models are based on spherical particles not taking into account specific interactions with surrounding solvent molecules. Simple molecular modeling using the MM3 force field [42–44] shows that $\{Ph_4[Y(DTTA)(H_2O)_2]^{-}{}_3\}$ is far from being a spherical compound (Fig. 11), and the calculated radii have to be taken as rough estimates.

It has been shown that addition of phosphate, an efficient disaggregation agent for π-stacking systems [61, 62], destroys the weak aggregates formed in solution. Attempts to destroy the aggregates of $\{Ph_4[Y(DTTA)(H_2O)_2]^{-}{}_3\}$ in concentrated solution failed owing to precipitation of the compound in the presence of phosphate buffer (5–250 equiv) (see the electronic supplementary material). Any attempt to measure directly the size of the aggregates using methods such as matrix-assisted laser desorption/ionization time-of-flight MS or dynamic light scattering did not succeed owing to the weak interaction leading to aggregation.

Conclusion

Ph_4DTTA_3 (**5**) has been designed as a mid-sized potential high-field MRI contrast agent which is able to bind three gadolinium ions. Its central core, composed of four benzene rings, was developed to form bigger entities by aggregation induced by intermolecular interactions through π-stacking. This compound has been successfully synthesized and purified despite two major difficulties: the presence of the disubstituted compound and its precipitation at $pH \leq 3$. The gadolinium complex $\{Ph_4[Gd(DTTA)(H_2O)_2]^{-}{}_3\}$ exhibits exceptionally high relaxivities of approximately 50 mM^{-1} s^{-1} (30 MHz, 25 °C) at gadolinium concentrations above 20 mM. The concentration dependence of the relaxivity of $\{Ph_4[Gd(DTTA)(H_2O)_2]^{-}{}_3\}$ gave the first clear evidence that this

compound forms aggregates in aqueous solution. To benefit from high relaxivity in in vivo applications, a local concentration of at least 3 mM Gd^{3+} (or 1 mM compound) should be attained.

Different theoretical approaches were used to fit simultaneously ^{17}O NMR and ^{1}H NMRD data of a concentrated sample as well as ^{1}H NMRD profiles measured at three Gd^{3+} concentrations. The fitted rotational correlations times as well as the Lipari–Szabo order parameter S^2 clearly increase with the concentration of the compound because of aggregation. This formation of aggregates was also established by a decrease of the self-diffusion constant. From the estimated mean radii of the agglomerates, it can be concluded that these are composed of two or a maximum of three monomers.

Interaction between the hydrophobic aromatic cores is evidenced by the ^{1}H NMR spectra of the diamagnetic analogue $\{Ph_4[Y(DTTA)(H_2O)_2]^-{}_3\}$. Presumably π-stacking of central aromatic cores is responsible for the formation of aggregates. The variation of the ^{1}H NMR spectra with temperature and concentration show that aggregation is dynamic and the equilibrium is shifted toward monomers at higher temperatures.

Acknowledgments We thank Luc Reymond and Kai Johnsson at EFPL for provision of the analytical and preparative HPLC systems and their numerous amounts of advice and many ideas. Kim von Allmen is thanked for the fastidious purifications and various types of assistance. Joël Teuscher and Catherine Schütz at EPFL are thanked for the time they devoted to the dynamic light scattering experiments. This work was supported by the Swiss National Science Foundation.

References

1. Trattnig S, Pinker K, Ba-Ssalamah A, Nöbauer-Huhmann I-M (2006) Eur Radiol 16:1280–1287
2. Helm L (2010) Future Med Chem 2:385–396
3. Vaughan T, DelaBarre L, Snyder C, Tian J, Akgun C, Shrivastava D, Liu W, Olson C, Adriany G, Strupp J, Andersen P, Gopinath A, van de Moortele P-F, Garwood M, Ugurbil K (2006) Magn Reson Med 56:1274–1282
4. Merbach AE, Helm L, Tóth É (eds) (2013) The chemistry of contrast agents in medical magnetic resonance imaging. Wiley, Chichester
5. Nonat AM, Gateau C, Fries PH, Helm L, Mazzanti M (2012) Eur J Inorg Chem 2012:2049–2061. doi: 10.1002/ejic.201101162
6. Costa J, Balogh E, Turcry V, Tripier R, Le Baccon M, Chuburu F, Handel H, Helm L, Tóth E, Merbach AE (2006) Chem Eur J 12:6841–6851
7. Livramento JB, Helm L, Sour A, O'Neil C, Merbach AE, Tóth É (2008) Dalton Trans 1195–1202
8. Miéville P, Jaccard H, Reviriego F, Tripier R, Helm L (2011) Dalton Trans 40:4260–4267
9. Mastarone DJ, Harrison VSR, Eckermann AL, Parigi G, Luchinat C, Meade TJ (2011) J Am Chem Soc 133:5329–5337
10. Costa J, Ruloff R, Burai L, Helm L, Merbach AE (2005) J Am Chem Soc 127:5147–5157
11. Livramento JB, Tóth É, Sour A, Borel A, Merbach AE, Ruloff R (2005) Angew Chem Int Ed 44:1480–1481
12. Livramento JB, Sour A, Borel A, Merbach AE, Tóth É (2006) Chem Eur J 12:989–1003
13. Moriggi L, Aebischer A, Cannizzo C, Sour A, Borel A, Bünzli J-CG, Helm L (2009) Dalton Trans 2088–2095
14. Tóth É, Vauthey S, Pubanz D, Merbach AE (1996) Inorg Chem 35:3375–3379
15. Lee T-M, Cheng TH, Ou MH, Chang CA, Liu G-C, Wang Y-M (2004) Magn Reson Chem 42:329–336
16. Platzek J, Niedballa U, Radüchel B (1996) DE 19508058:13
17. Elmorsy SS, Pelter A, Smith K (1991) Tetrahedron Lett 32:4175–4176
18. Plater MJ (1993) Synlett 405–406
19. Cherioux F, Guyard L (2001) Adv Funct Mater 11:305–309
20. Xia H, He J, Peng P, Zhou Y, Li Y, Tian W (2007) Tetrahedron Lett 48:5877–5881
21. Corsi DM, Platas-Iglesias C, Van Bekkum H, Peters JA (2001) Magn Reson Chem 39:723–726
22. Lide DR (ed) (2007) Handbook of chemistry and physics, 88th edn. CRC, Boca Raton
23. Ferrante G, Sykora S (2005) In: van Eldik R, Bertini I (eds) Advances in inorganic chemistry, vol 57. Elsevier, San Diego, pp 405–470
24. Ammann C, Meier P, Merbach AE (1982) J Magn Reson 46:319–321
25. Li L, Sotak CH (1991) J Magn Reson 92:411
26. Vold RL, Waugh JS, Klein MP, Phelps DE (1968) J Chem Phys 48:3831–3832
27. Meiboom S, Gill D (1958) Rev Sci Instrum 29:688–691
28. Solomon I (1955) Phys Rev 99:559–565
29. Bloembergen N (1957) J Chem Phys 27:572–573
30. Bloembergen N (1957) J Chem Phys 27:595
31. Lipari G, Szabo A (1982) J Am Chem Soc 104:4546–4559
32. Lipari G, Szabo A (1982) J Am Chem Soc 104:4559–4570
33. Rast S, Fries PH, Belorizky E (2000) J Chem Phys 113:8724–8735
34. Rast S, Borel A, Helm L, Belorizky E, Fries PH, Merbach AE (2001) J Am Chem Soc 123:2637–2644
35. Yerly F (2002) Optimiseur 3.0.0. EPFL, Lausanne
36. Yerly F (2004) Visualiseur 2.3.6. EPFL, Lausanne
37. Bertini I, Kowalewski J, Luchinat C, Nilsson T, Parigi G (1999) J Chem Phys 111:5795–5807
38. Kruk D, Nilsson T, Kowalewski J (2001) Phys Chem Chem Phys 3:4907
39. Kowalewski J, Kruk D, Parigi G (2005) In: Van Eldik R, Bertini I (eds) Advances in inorganic chemistry, vol 57. Elsevier, San Diego, pp 41–104
40. Bertini I, Galas O, Luchinat C, Parigi G (1995) J Magn Reson A 113:151–158
41. Caravan P, Parigi G, Chasse JM, Cloutier NJ, Ellison JJ, Lauffer RB, Luchinat C, McDermid SA, Spiller M, McMurry TJ (2007) Inorg Chem 46:6632–6639
42. Allinger NL, Yuh YH, Lii J-H (1989) J Am Chem Soc 111:8551–8566
43. Lii J-H, Allinger NL (1989) J Am Chem Soc 111:8566–8575
44. Lii J-H, Allinger NL (1989) J Am Chem Soc 111:8575–8582
45. Moriggi L, Cannizzo C, Prestinari C, Berrière F, Helm L (2008) Inorg Chem 47:8357–8366
46. Woessner DE (1996) In: Grant DM, Harris RK (eds) Encyclopedia of nuclear magnetic resonance. Wiley, Chichester, pp 1068–1084
47. Powell DH, Ni Dhubhghaill OM, Pubanz D, Helm L, Lebedev YS, Schlaepfer W, Merbach AE (1996) J Am Chem Soc 118:9333–9346
48. Hwang LP, Freed JH (1975) J Chem Phys 63:4017–4025

49. Freed JH (1978) J Chem Phys 69:4034–4037
50. Ayant Y, Belorizky E, Alizon J, Gallice J (1975) J Phys 36:991–1004
51. Belorizky E, Fries PH, Helm L, Kowalewski J, Kruk D, Sharp RR, Westlund P-O (2008) J Chem Phys 128:052307
52. Dunand FA, Tóth É, Hollister R, Merbach AE (2001) J Biol Inorg Chem 6:247–255
53. Kowalewski J, Luchinat C, Nilsson T, Parigi G (2002) J Phys Chem A 106:7376–7382
54. Dunand FA, Borel A, Merbach AE (2002) J Am Chem Soc 124:710–716
55. Dunand FA, Borel A, Helm L (2002) Inorg Chem Commun 5:811–815
56. Yazyev OV, Helm L, Malkin VG, Malkina OL (2005) J Phys Chem A 109:10997–11005
57. Helm L (2006) Prog NMR Spectrosc 49:45–64
58. Costa J, Tóth É, Helm L, Merbach AE (2005) Inorg Chem 44:4747–4755
59. Johnson CS Jr (1999) Prog NMR Spectrosc 34:203–256
60. Morris KF, Johnson CS Jr (1992) J Am Chem Soc 114:3139–3141
61. Laus S, Sitharaman B, Tóth É, Bolskar RD, Helm L, Asokan S, Wong MS, Wilson LJ, Merbach AE (2005) J Am Chem Soc 127:9368–9369
62. Laus S, Sitharaman B, Tóth É, Bolskar RD, Helm L, Wilson LJ, Merbach AE (2007) J Phys Chem C 111:5633–5639